Turkish Journal of Physics

http://journals.tubitak.gov.tr/physics/

Research Article

Turk J Phys
(2018) 42: 368 – 377

doi:10.3906/fiz-1802-21

An experimental study on the angular dependence of coherent to Compton scattering differential cross-section ratios of calcium

Tuba AKKUŞ*
Department of Physics, Faculty of Arts and Sciences, Erzincan Binali Yıldırım University, Erzincan, Turkey

Received: 12.02.2018 • **Accepted/Published Online:** 30.05.2018 • **Final Version:** 15.08.2018

Abstract: The coherent to Compton scattering cross-section ratio of calcium was measured experimentally for several polar scattering angles (90°, 100°, 110°, 120°, and 130°) and azimuthal scattering angles (30°, 20°, 10°, 0°, −10°, and −20°). A high purity germanium semiconductor detector with a resolution of 199.6 eV at 5.9 keV was used. The theoretical values of the coherent to Compton scattering differential cross-section of calcium were calculated on the basis of nonrelativistic form factors, relativistic form factors, and S-matrix theories. It was observed that the experimental results were most compatible with the nonrelativistic form factor theory.

Key words: Atomic form factors, coherent to Compton scattering cross-section ratio, differential cross-section, angular dependence, azimuthal angle

1. Introduction

The fundamental interactions between matter and X-rays with energy values of less than 1 MeV are coherent (Rayleigh) scattering, incoherent (Compton) scattering, and photoelectric absorption. In the photoelectric absorption process, a photon interacts with a bound atomic electron in such a way that it loses all of its energy. Some of the photon energy is used to overcome the binding energy, and most of the remainder is transferred to the free electron as kinetic energy [1].

Two different scatterings are observed during the interaction of the photons with the matter. These scatterings are coherent and incoherent scattering. Rayleigh or coherent scattering is an interaction between an atom and low energy photons. In this case, the atom is neither ionized nor excited. Compton or incoherent scattering occurs as a consequence of atomic free electron interaction with a photon [2].

Coherent and Compton scattered lines can be found together with fluorescent lines in an XRF spectrum. Compton scattering is observed in elements with very low atomic number while Rayleigh scattering is observed in elements with higher atomic numbers.

Therefore, the intensity ratio of the coherent to Compton scattering should be sensitive to small changes in the composition of the samples [3].

Differential cross-section is defined as the cross-section per unit solid angle. A majority of the differential cross-sections are usually explained by angular distribution since they are dependent on the interaction (incoming and outgoing) angle. The differential cross-section is an extremely useful quantity in many fields of physics, such as reactor shielding, medical physics, space physics, and plasma physics.

*Correspondence: takkus@erzincan.edu.tr

A lot of experimental results on coherent differential cross-sections [4–6], Compton differential cross-sections [7–9], and coherent to Compton differential cross-section ratios [10–17] have been reported in the literature.

There are numerous studies in the literature on the polar scattering angle dependence of coherent to Compton differential cross-sections. The objective of the present study was to measure the coherent to Compton differential cross-section ratios of calcium with different polar and azimuthal angles.

2. Theory

Rayleigh scattering usually occurs in materials with low energy and high atomic number. The differential Rayleigh scattering cross-section for unpolarized photons is expressed as [18]

$$\frac{d\sigma_{coh}}{d\Omega} = \frac{r_0^2}{2}\left(1+\cos^2\theta\right)\left|F\left(x,Z\right)\right|^2, \tag{1}$$

where r_0, $F\left(x,Z\right)$, Z, and x represent the classical electron radius, atomic form factor atomic number, and momentum transfer parameter, respectively. The momentum transfer parameter is expressed as

$$x = \left(Sin\theta/2\right)/\lambda\left(\mathring{A}\right), \tag{2}$$

where λ (Å) is usually given in angstroms and represents the wavelength of the incoming photon, which can be given as 12398.520 / E (eV), while θ denotes the angle between the incoming photon direction and scattered photon direction.

In the present study, λ was 0.208 Å and the values of momentum transfer parameters corresponding to 90°, 100°, 110°, 120°, and 130° scattering angles were 3.399, 3.683, 3.938, 4.164, and 4.357 Å^{-1} respectively.

The differential inelastic cross-section for a single free electron is given by the Klein–Nishina [19] collision cross-section $d\sigma_{KN}\left(\theta\right)/d\Omega$ for unpolarized photons striking unbound, randomly oriented electrons:

$$\frac{d\sigma_{KN}\left(\theta\right)}{d\Omega} = \frac{r_0^2}{2}P\left(\theta,E\right), \tag{3}$$

where $P\left(\theta,E\right)$ is the polarization factor and can be expressed as

$$P(\theta,E) = \left[\frac{1}{1+\alpha\left(1-\cos\theta\right)}\right]^2\left[1+\cos^2\theta+\frac{\left[\alpha^2\left(1-\cos\theta\right)^2\right]}{1+\alpha\left(1-\cos\theta\right)}\right], \tag{4}$$

where $\alpha = E/m_0c^2$. If α is very small, that is, if the photon energy is much smaller than the electron rest mass, then the polarization factor reduces to $1+\cos^2\theta$ and the Klein–Nishina differential cross-section reduces to the Thomson one. In order to account for the interference between the waves scattered by each electron in the atom, the incoherent scattering function $S(x,Z)$ has been introduced. Scattering from the bound electrons is given by the following equality:

$$\frac{d\sigma_{Comp}}{d\Omega} = \frac{d\sigma_{KN}}{d\Omega}S\left(x,Z\right), \tag{5}$$

where $S\left(x,Z\right)$ represents the incoherent scattering function.

The nonrelativistic form factor (NRFF) [20], relativistic form factor (RFF) [21], and S-matrix theory [22] were used for theoretical calculations in the present study. The values of $S(x,Z)$ and $F(x,Z)$ have been tabulated and extrapolated by Hubbell et al. [20] using nonrelativistic Hartree–Fock atomic wave functions. The relativistic wave function was used by Hubbell and Overbo [21]. Lastly, the work of Chatterjee and Roy is used for S-matrix formulations in electrodynamics [22].

3. Experimental

The experimental setup used in the present study is shown in Figure 1. The polar and azimuthal scattering angles were measured within the range of $90^\circ \leq \theta \leq 130^\circ$ and $+30^\circ \leq \phi \leq -20^\circ$, respectively, with steps of 10°. The source and target were rotated together around the z axis in all measurements. The detector was kept at the same position during the measurements. The detector was shielded by a lead collimator to avoid direct exposure to incoming radiation from the source and environment. An Am^{241} radioactive point source with 100 mCi activity was used to irradiate the samples. The emitted X-rays and scattered photons were detected using a high purity germanium detector with a resolution of 199.6 eV at 5.9 keV, an active area of 200 mm^2, and a beryllium window of 12.5 μm thickness.

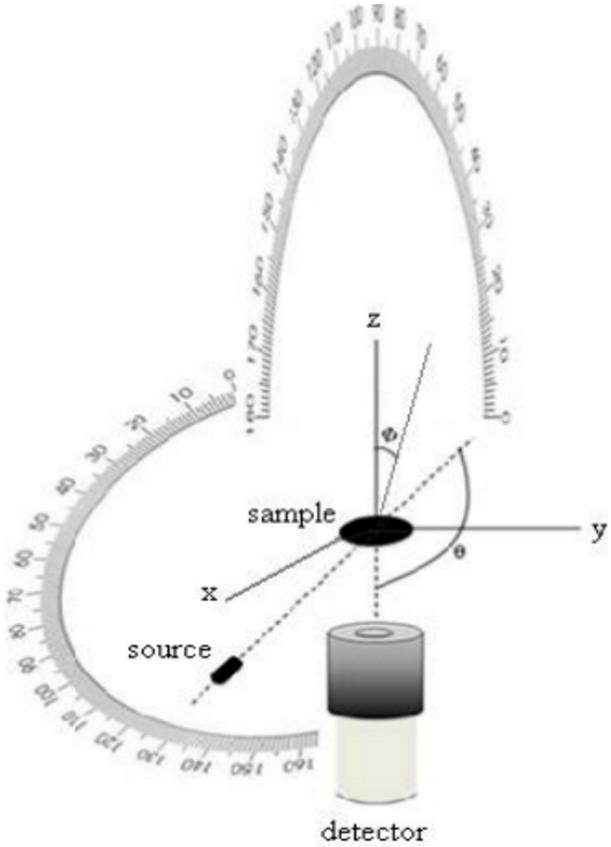

Figure 1. Experimental geometry for the determination of the angular dependence of coherent to Compton scattering differential cross-section ratios of calcium. ϕ is azimuthal angle, θ is polar angle.

A software program was used to acquire the spectra and to control the operating parameters of the system. The data were entered into 4096 channels of the multichannel analyzer. A computer program was used

to determine the net peak areas. The typical spectrum of the calcium target at various polar and azimuthal scattering angles is shown in Figure 2.

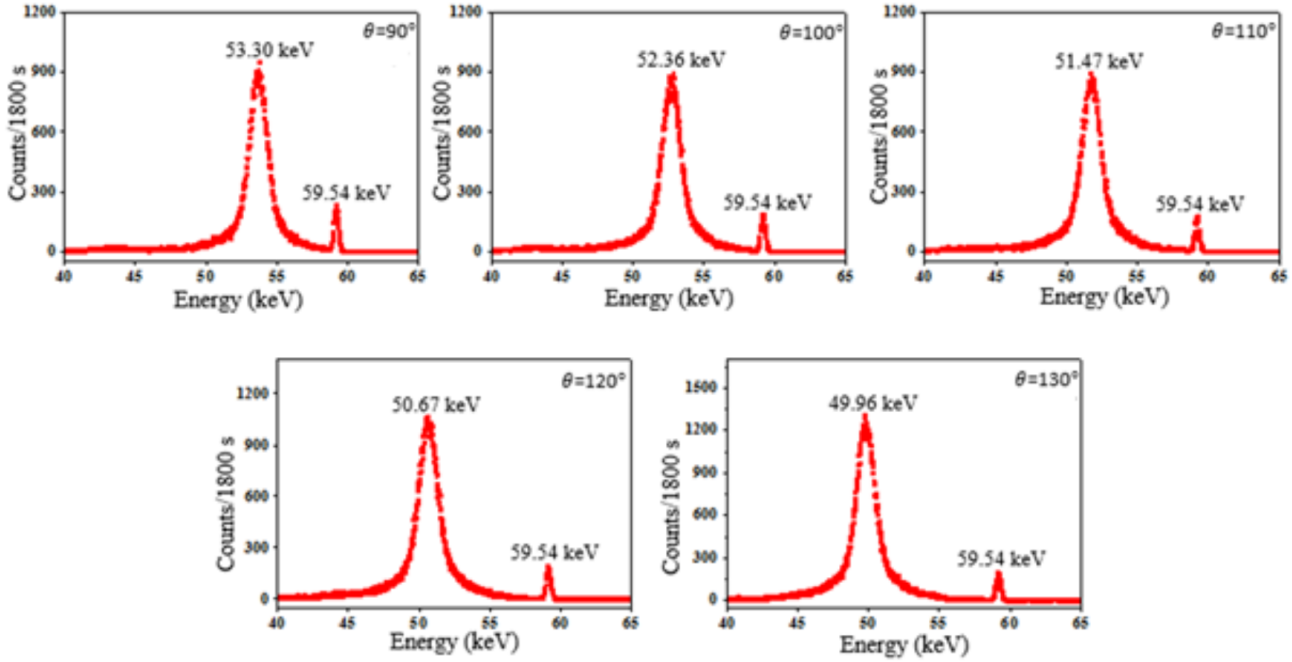

Figure 2. The variation of the Compton peak energy at various polar scattering angles.

The experimental coherent to Compton scattering differential cross-section ratio is given by [15]:

$$\frac{d_{coh}}{d_{Comp}} = \frac{N_{coh}}{N_{Comp}} \frac{\beta_{\gamma t(Comp)}}{\beta_{\gamma t(coh)}} \frac{\beta_{\gamma a(Comp)}}{\beta_{\gamma a(coh)}} \frac{\varepsilon_{\gamma(Comp)}}{\varepsilon_{\gamma(coh)}}, \tag{6}$$

where N_{coh}/N_{Comp} is the ratio of the number of counts under the coherent and Compton scattering peaks, $\beta_{\gamma t(Comp)}/\beta_{\gamma t(coh)}$ is the ratio of self-absorption correction factors in the target for Compton and coherent scattered photons, $\beta_{\gamma a(Comp)}/\beta_{\gamma a(coh)}$ is the ratio of the air absorptions for Compton scattered and coherent scattered gamma rays in air, and $\varepsilon_{\gamma(Comp)}/\varepsilon_{\gamma(coh)}$ is the ratio of photo peak efficiencies of the high purity germanium detector for Compton and coherent scattered photons.

The self-absorption and air absorption correction factors were calculated via Eqs. (7) and (8), respectively:

$$\beta_{\gamma t} = \frac{1 - \exp\left[(-1)\left(\frac{\mu_i}{\cos\theta_1} + \frac{\mu_s}{\cos\theta_2}\right) t_t\right]}{\left(\frac{\mu_i}{\cos\theta_1} + \frac{\mu_s}{\cos\theta_2}\right) t_t}, \tag{7}$$

$$\beta_{\gamma a} = \frac{1 - \exp\left[(-1)\left(\frac{\mu_i}{\cos\theta_1} + \frac{\mu_s}{\cos\theta_2}\right) t_a\right]}{\left(\frac{\mu_i}{\cos\theta_1} + \frac{\mu_s}{\cos\theta_2}\right) t_a}, \tag{8}$$

where μ_i and μ_s are the mass attenuation coefficients at the incident photon energy and incoherently scattered photon energy, respectively. The values of mass attenuation coefficients were taken from Winxcom [23]. t_t and

t_a are the mass thicknesses of the sample and air, respectively. θ_1 and θ_2 are the angles of the incident and scattered γ rays with the target normal.

The effective incident photon flux factor $I_0 G\varepsilon$ is generally determined by using the number of counts under the K_β or K_α peaks but in this study the photo peak efficiency curve for the high purity germanium detector curve was obtained experimentally in the range of 26.35–661.66 keV photon energy by using Am^{241}, Ba^{133}, Eu^{152}, and Cs^{137} radioactive calibration sources. This is a more convenient method since Compton and coherent peaks are found in the high energy region of the spectrum.

The radioactive sources were placed on the location of the sample for efficiency calculations, after which the spectra were recorded. Efficiency calculation using radioactive sources is carried out as follows [15]:

$$\varepsilon_\gamma = \frac{A_C}{N_\lambda P_\gamma}, \tag{9}$$

where A_C, N_λ, and P_γ are the net peak area in counts, the activity of the source at the time of standardization, and the absolute gamma ray emission probability, respectively. The activity of the radioactive source can be calculated from the known decay law,

$$N_\lambda = N_0 e^{-\lambda_d t}, \tag{10}$$

where N_0 is the initial activity of the radioactive source, λ^d is the decay constant, and t is the elapsed time. The decay constant can be easily found since the half-life of radioactive sources is known:

$$\lambda^d = 0.693/t_{1/2}. \tag{11}$$

The photo peak efficiency curve obtained from the above equations is given in Figure 3.

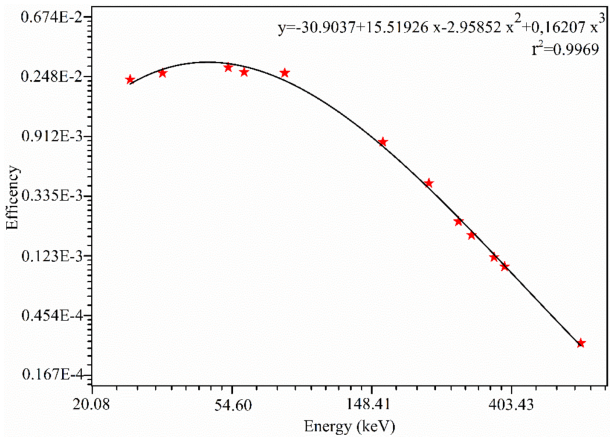

Figure 3. The experimental photopeak efficiency curve for high purity germanium detector.

4. Results

The variation of Compton peak energy with the changing scattering angle is shown in Figure 2. The energy of Compton scattered gamma rays can be found using the well-known Compton scattering equation,

$$E = \frac{E_0}{1 + \left(\frac{E_0}{m_e c^2}\right)(1 - \cos\theta)}, \tag{12}$$

where E_0 is the incident photon energy, m_e is the electron mass, c is the speed of light in vacuum, and θ is the scattering angle. The coherent to Compton scattering ratio is a very useful method for trace element analysis because a number of parameters such as absolute source strength, solid angles subtended by source, and detector at the target are eliminated in the expression of coherent to Compton ratio; otherwise, determination of these parameters introduces a large amount of error in the results [14].

The calculated experimental and theoretical values of coherent to Compton differential cross-section ratios of calcium are given in the Table. The theoretical results are given only at an azimuthal scattering angle of 0° because there are no data on the azimuthal angles of 30°, 20°, 10°, -10°, and -20° for calcium. The experimental calculation is carried out as mentioned in the experimental section.

The dependence of the coherent to Compton differential cross-sections on scattering angle is given in Figures 4–8. As can be seen in these figures, there is a good third order polynomial relation between the differential cross-section and scattering angles. As expected, coherent to Compton scattering differential cross-section ratios decrease with increasing scattering angles.

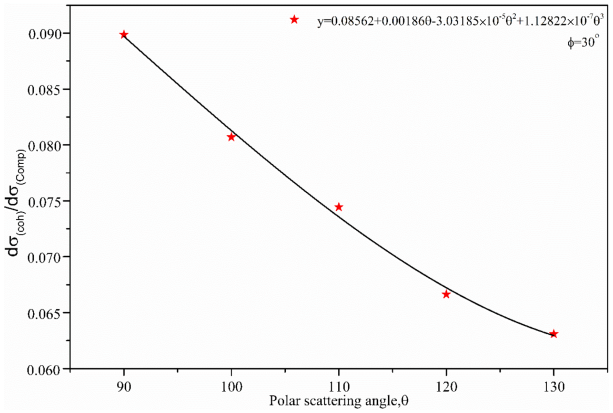

Figure 4. Variation of the coherent to Compton differential cross-section ratios at the azimuthal scattering angle of 30° for various polar scattering angles.

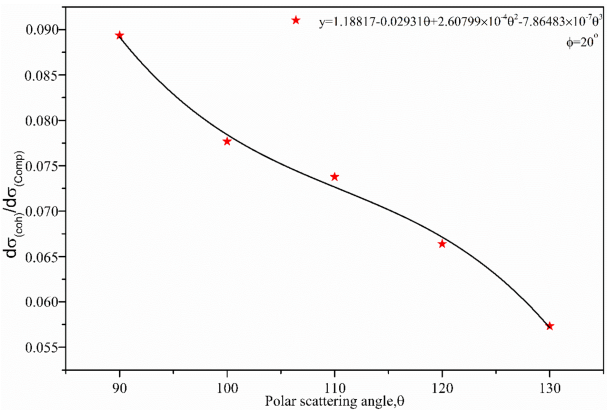

Figure 5. Variation of the coherent to Compton differential cross-section ratios at the azimuthal scattering angle of 20° for various polar scattering angles.

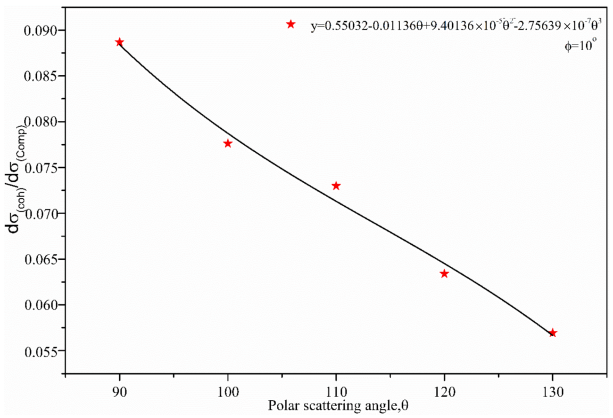

Figure 6. Variation of the coherent to Compton differential cross-section ratios at the azimuthal scattering angle of 10° for various polar scattering angles.

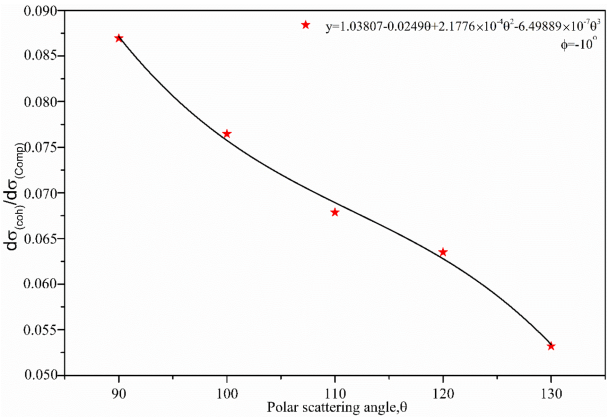

Figure 7. Variation of the coherent to Compton differential cross-section ratios at the azimuthal scattering angle of -10° for various polar scattering angles.

Table. Experimental and theoretical values of the coherent to incoherent scattering cross-section ratios of calcium for various polar and azimuthal scattering angles. T^n, T^r, and T^s are the theoretical values calculated from the nonrelativistic form factor theory, relativistic form factor theory, and S-matrix theory, respectively.

Scattering angle (θ)	Azimuthal angle (ϕ)								
	$+30^\circ$	$+20^\circ$	$+10^\circ$	0°				-10°	-20°
	Experimental				T^n	T^r	T^s	Experimental	
90°	0.0898 ±0.0029	0.0893 ±0.0026	0.0887 ±0.0021	0.0876 ±0.0023	0.0785	0.0783	0.0754	0.0869 ±0.0023	0.0849 ±0.0029
100°	0.0807 ±0.0027	0.0777 ±0.0023	0.0776 ±0.0023	0.0765 ±0.0022	0.0692	0.0695	0.0668	0.0764 ±0.0024	0.0751 ±0.0026
110°	0.0744 ±0.0022	0.0738 ±0.0025	0.0073 ±0.0022	0.0684 ±0.0021	0.0626	0.0624	0.0599	0.0678 ±0.0020	0.0669 ±0.0017
120°	0.0666 ±0.0019	0.0664 ±0.0020	0.0634 ±0.0019	0.0654 ±0.0019	0.0572	0.0568	0.0544	0.0635 ±0.0019	0.0615 ±0.0020
130°	0.0631 ±0.0021	0.0573 ±0.0013	0.0569 ±0.0019	0.0547 ±0.0011	0.0527	0.0524	0.0500	0.0532 ±0.0018	0.0518 ±0.0013

As can be seen in Figure 9, coherent to incoherent scattering differential cross-section ratios increase with the increasing values of the azimuthal angle for each fixed polar scattering angle.

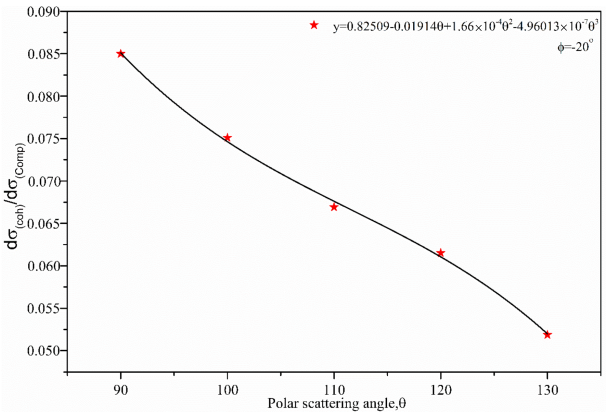

Figure 8. Variation of the coherent to Compton differential cross-section ratios at the azimuthal scattering angle of -20° for various polar scattering angles.

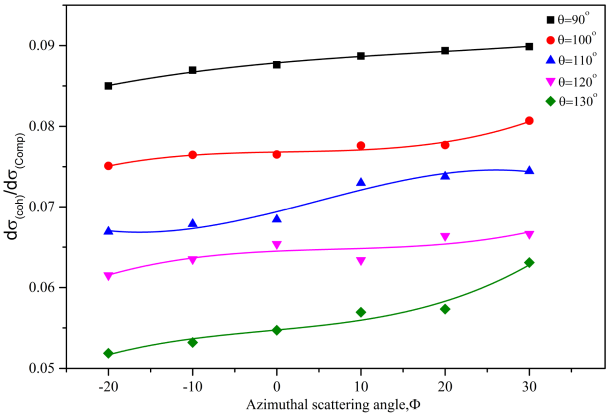

Figure 9. Variation of the coherent to incoherent differential cross-section ratios with the azimuthal angle at the fixed polar scattering angles.

The experimental and theoretical results at an azimuthal scattering angle of 0° are given in Figure 10 for easier observation and comparison. It can be seen that the experimental results are greater than those obtained with different theoretical approaches. The experimental results were determined to be greater than the theoretical results in our previous study [15].

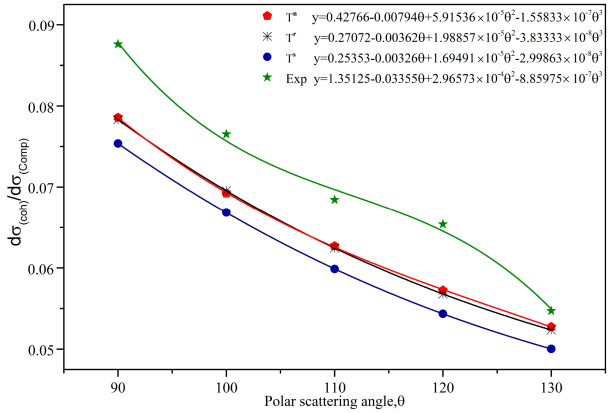

Figure 10. Variation of the coherent to Compton scattering cross-section ratio as function of scattering angle along with the theoretical data for azimuthal angle of 0°. Exp represents the experimental values; T^n, T^r, and T^s represent the theoretical values calculated from the nonrelativistic form factor theory, relativistic form factor theory, and S-matrix theory, respectively.

The uncertainty calculation for coherent to Compton scattering differential cross-section ratios can be given as:

$$\Delta\left(\frac{d\sigma_{coh}}{d\sigma_{Comp}}\right)=\left[\left(\frac{\Delta N_{(coh)}}{N_{(coh)}}\right)^2+\left(\frac{\Delta N_{(Comp)}}{N_{(Comp)}}\right)^2+\left(\frac{\Delta\beta_{\gamma t(Comp)}}{\beta_{\gamma t(Comp)}}\right)^2+\left(\frac{\Delta\beta_{\gamma t(coh)}}{\beta_{\gamma t(coh)}}\right)^2+\left(\frac{\Delta\beta_{\gamma a(Comp)}}{\beta_{\gamma a(Comp)}}\right)^2\right.$$
$$\left.+\left(\frac{\Delta\beta_{\gamma a(coh)}}{\beta_{\gamma a(coh)}}\right)^2+\left(\frac{\Delta\varepsilon_{\gamma(coh)}}{\varepsilon_{\gamma(coh)}}\right)^2+\left(\frac{\Delta\varepsilon_{\gamma(Comp)}}{\varepsilon_{\gamma(Comp)}}\right)^2\right]^{1/2},$$

where $\Delta N_{(coh)}$, $\Delta N_{(Comp)}$, $\Delta\beta_{\gamma t(Comp)}$, $\Delta\beta_{\gamma t(coh)}$, $\Delta\beta_{\gamma a(Comp)}$, $\Delta\beta_{\gamma a(coh)}$, $\Delta\varepsilon_{\gamma a(coh)}$, and $\Delta\varepsilon_{\gamma(Comp)}$ are the errors in the intensities $N_{(coh)}$ and $N_{(Comp)}$, self-absorption correction factors $\beta_{\gamma t(Comp)}$ and $\beta_{\gamma t(coh)}$, air absorption correction factors $\beta_{\gamma a(Comp)}$ and $\beta_{\gamma a(coh)}$, $\varepsilon_{\gamma(coh)}$, and $\varepsilon_{\gamma(Comp)}$ efficiencies, respectively.

The discrepancies between the experimental and theoretical values are within the ranges of 3.72%–14.22%, 4.49%–15.13%, and 9.35%–20.28% for the nonrelativistic form factor theory (T^n), relativistic form factor theory (T^r), and S-matrix theory (T^s), respectively.

There is a clear agreement between the experimental values and the results of the nonrelativistic form factor theory in comparison with the relativistic form factor theory and S-matrix theory.

5. Conclusion

The coherent to Compton scattering cross-section ratio of calcium was calculated experimentally for various polar and azimuthal scattering angles in this study. The results obtained were compared with three different theoretical results.

It was observed that the angular distributions of coherent to Compton scattering differential cross-section ratios were examined only in polar or azimuthal angles and there was no experimental study in the literature that investigates both the azimuthal and polar angular distribution. Thus, the objective of this study was to provide a spatial mapping of the angular dependence of coherent to Compton scattering differential cross-section ratios.

The theoretical results do not contain the binding force or binding energy of the electrons and it was assumed that Compton scattering occurs as a result of the interaction between the incoming photon and free electron.

References

[1] Nelson, G.; Reilly, D. *Passive Nondestructive Analysis of Nuclear Materials*; Los Alamos National Laboratory: Los Alamos, NM, USA, 1991.

[2] Van Grieken, R. E.; Markowicz, A. A. *Handbook of X-ray Spectrometry*; Marcel Dekker: New York, NY, USA, 2001.

[3] Li, F.; Liu, Z.; Sun, T. *Food Chem*. **2016**, *210*, 435-441.

[4] Erzeneoglu, S.; Demir, L.; Sahin, Y. *Phys. Scripta* **1997**, *56*, 89-91.

[5] Şimşek, Ö. *Nucl. Instrum. Meth. B* **2000**, *160*, 7-10.

[6] İçelli, O.; Erzeneoğlu, S. *Spectrochim. Acta B* **2001**, *56*, 331-335.

[7] Shahi, J. S.; Kumar, A.; Mehta, D.; Puri, S.; Garg, M. L., Singh, N. *Nucl. Instrum. Meth. B* **2001**, *179*, 15-23.

[8] Kurucu, Y. *J. Electron. Spectrosc.* **2005**, *142*, 39-43.

[9] Boke, A. *Radiat. Phys. Chem.* **2013**, *83*, 34-41.

[10] İcelli, O.; Erzeneoglu, S. *Spectrochim. Acta B* **2002**, *57*, 1317-1323.

[11] Simsek, O.; Ertugrul, M.; Budak, G.; Karabulut, A. *X-ray Spectrom.* **2004**, *33*, 349-353.

[12] Singh, M. P.; Sandhu, B. S.; Singh, B. *Phys. Scripta* **2007**, *76*, 281-286.

[13] Singh, M. P.; Sharma, A.; Singh, B.; Sandhu, B. S. *Indian J. Pure Ap. Phy.* **2012**, *50*, 490-493.

[14] Singh, M. P.; Sharma, A.; Singh, B.; Sandhu, B. S. *Radiat. Meas.* **2013**, *59*, 30-36.

[15] Akkuş, T.; Pirimoğlu Dal, M.; Şahin, Y. *Radiat. Phys. Chem.* **2015**, *117*, 167-171.

[16] Boydaş, E.; Yılmaz, D.; Cömert, E. *Instrum. Sci. Technol.* **2016**, *44*, 642-650.

[17] Yılmaz, D.; Şimşek, Ü.; Akkuş, T.; Şahin, Y. *Can. J. Phys.* **2017**, *95*, 407-411.

[18] Pirienne, M. N. *The Diffraction of X-rays and Electrons by Free Molecules*; Cambridge University Press: New York, NY, USA, 1946.

[19] Klein, O.; Nishina, Y.; Von Dirac. *Z. Phys.* **1929**, *52*, 853-868.

[20] Hubbell, J. H.; Viegele, W. J.; Biggs, E. A.; Brown, R. T.; Cromer, D. T.; Howerton, R. J. *J. Phys. Chem. Ref. Data* **1975**, *4*, 471-498.

[21] Hubbell, J. H.; Overbo, I. *J. Phys. Chem. Ref. Data* **1979**, *8*, 69-105.

[22] Chatterjee, B. K.; Roy, S. C. *J. Phys. Chem. Ref. Data* **1998**, *27*, 1011-1215.

[23] Gerward, L.; Guilbert, N.; Jensen, B. K.; Levring, H. *Radiat. Phys. Chem.* **2001**, *60*, 23-24.